[redacted]

TM X-59750

A COMPARISON OF HUMAN RESPONSE MODELING IN THE TIME AND FREQUENCY DOMAINS

By Lawrence W. Taylor, Jr.
NASA Flight Research Center
Edwards, Calif.

Presented at the
USC/NASA Conference on Manual Control
Los Angeles, Calif.
March 1-3, 1967

PREPRINT

A COMPARISON OF HUMAN RESPONSE MODELING IN THE TIME AND FREQUENCY DOMAINS

By Lawrence W. Taylor, Jr.
NASA Flight Research Center
Edwards, Calif.

SUMMARY

Frequency and time domain methods of analyzing human control response while performing compensatory tracking tasks are reviewed. Sample linear model results using these methods are compared and discussed. The inherent requirement of constraining the freedom of the form of the pilot models is also discussed. The constraint in the frequency domain consists of smoothing with respect to frequency; whereas, the constraint for the time domain model is more natural and meaningful in that it consists simply of limiting the memory of the pilot model. The linear models determined by both methods were almost identical.

The time domain method of analysis enables the determination of a nonlinear pilot model. The inclusion of a cubic as well as a linear term accounted for only a small additional part of the pilot's remnant and indicated that only a small portion of the total power of the pilot's output is caused by nonlinearities. The power-spectral density of an ensemble average of the pilot's output is used to determine the upper limit of the amount of power associated with a deterministic response. The indication is that more than half the remnant is stochastic when a linear model is used.

INTRODUCTION

Since the MIT-NASA Working Conference on Manual Control at Cambridge, Mass., February 28-March 2, 1966, additional work in human response analysis, both theoretical and experimental, has been performed at the NASA Flight Research Center. Much of this work has been part of a continuation of a NASA-USAF-Cornell Aeronautical Laboratory program to obtain pilot describing functions from both flight and simulator tests. In addition to this program, the Flight Research Center has initiated a study, under the guidance of Dr. A. V. Balakrishnan of UCLA, of nonlinear time domain methods as applied to the problem of modeling the pilot in a compensatory tracking task.

It is the purpose of this paper to assess first the frequency domain method of analysis and then the time domain analysis. A comparison of the results of the two forms of analysis applied to a linear model is made, and their advantages and disadvantages are discussed. Next, the time domain method of analysis is applied to the identification of a nonlinear pilot model. This is the first time that the nonlinear time domain method has been applied to human response data. The power-spectral density of an ensemble average of the pilot's output is used to estimate the amounts of power that correspond to linear, deterministic, and stochastic control response.

DESCRIPTION OF EXPERIMENT

The classical experiment for obtaining data from which pilot models can be identified is illustrated in figure 1. The pilot is asked to minimize the error, e, displayed to him by an oscilloscope, television screen, or meter by manipulating a controller. The controller deflection, c, is sent to an analog computer which computes the response of the controlled element and adds to it the input disturbance function, i, forming an error which, in turn, is sent to the display. The signals are either processed during the experiment or recordings are made of the signals which are later processed to obtain the model of the pilot (ref. 1). Similar experiments have been performed in flight in which the pilot maneuvers the airplane (refs. 2 and 3). Most of the data analyzed in this paper were collected as part of the joint NASA-USAF-Cornell Aeronautical Laboratory human response studies (ref. 3) involving the T-33 variable-stability airplane and ground simulators.

DISCUSSION AND RESULTS

Frequency Domain Methods

Classically, the model of the pilot is considered to be a linear-describing function with output, o, plus a remnant signal, r, as shown in figure 2. The describing function, $Y_p(j\omega)$, can be obtained by first computing the cross-spectral density functions $\Phi_{ic}(j\omega)$ and $\Phi_{ie}(j\omega)$. The estimate of $Y_p(j\omega)$ is then given by the ratio (from ref. 4)

$$\hat{Y}_p(j\omega) = \frac{\Phi_{ic}(j\omega)}{\Phi_{ie}(j\omega)}$$

Cross-spectral density functions have generally been used instead of Fourier transforms (ref. 5) as a means of removing the bias in the estimate of $Y_p(j\omega)$ introduced by the remnant. The use of cross-spectral density functions, however, was shown in reference 6 to have no effect on the bias. The same estimate of $Y_p(j\omega)$, therefore, can be expressed as the ratio of Fourier transforms

$$\hat{Y}_p(j\omega) = \frac{F[c(t)]}{F[e(t)]}$$

and the bias in both cases is

$$\hat{Y}_p(j\omega) - Y_p(j\omega) = \frac{\Phi_{ir}(j\omega)}{\Phi_{ie}(j\omega)} = \frac{F[r(t)]}{F[e(t)]}$$

These conclusions, which were developed in reference 6, depend on the ability to express the cross-spectral density in terms of Fourier transforms. Appendix A contains a detailed mathematical proof of the expression, and appendix B presents experimental results which further substantiate these conclusions.

The frequency domain method of analysis was used in the human control response study of reference 3 in which compensatory tracking experiments were performed in flight and on simulators. Figure 3 shows some simulator results in which the values presented for $\hat{Y}_p(j\omega)$ are the means of 10 runs for pilot A and three runs each for pilots B and C. The vertical lines indicate the range of plus or minus one sigma for each of the points. The lack of a vertical line indicates the range to be less than the height of the symbol. The input disturbance function consisted of the sum of 10 sinusoids. Values of $\hat{Y}_p(j\omega)$ were determined at the input frequencies. The use of sinusoids for the input disturbance function has the advantage of concentrating the power at several frequencies, thereby enhancing the accuracy of the estimate of the pilot describing function at the input frequencies.

If, on the other hand, a random input is used, mathematical difficulties may be encountered when using frequency domain methods. For example, if no constraint is placed on the form of $Y_p(j\omega)$, the resulting estimate will account for the entire pilot output, c, erroneously indicating the remnant, r, to be zero. This result comes from applying the relationship

$$\hat{Y}_p(j\omega) = \frac{\Phi_{ic}(j\omega)}{\Phi_{ie}(j\omega)} = \frac{F[c(t)]}{F[e(t)]}$$

at all frequencies. Figure 4 shows an example of the erratic function (dashed lines) that results from such a procedure. A constraint on $\hat{Y}_p(j\omega)$ is usually provided by smoothing the values of the cross-spectral density functions or Fourier transforms, or by fairing a curve through the raw estimates of the pilot's describing function, $\hat{Y}_p(j\omega)$, or both. Nevertheless, the required constraint on $\hat{Y}_p(j\omega)$ compromises one of the claims made for the analyses in the frequency domain, namely, that of unlimited freedom in model representation. Also indicated in figure 4 is the effect of smoothing on the average linear coherence, ρ_a. The value is seen to change from 1.0, for the raw estimates, to 0.91 for the faired case. The value of ρ_a or any other measure of the remnant has meaning only when connected to some particular pilot-constrained model.

If the raw cross spectral densities are smoothed, the estimate of Y_p becomes

$$\hat{Y}_p(j\omega) = \frac{\sum_{k=-K}^{K} W_k \Phi_{ic}(j\omega + jk\Delta\omega)}{\sum_{k=-K}^{K} W_k \Phi_{ie}(j\omega + jk\Delta\omega)}$$

This estimate can also be expressed in terms of Fourier transforms as

$$\hat{Y}_p(j\omega) = \frac{\sum_{k=-K}^{K} W_k F_k^*[i(t)]\, F_k[c(t)]}{\sum_{k=-K}^{K} W_k F_k^*[i(t)]\, F_k[e(t)]}$$

It should be noted that although the smoothing is indicated to be in the frequency domain the same result can be obtained by averaging or truncation in the time domain.

Another point made in reference 6 is that the correlation coefficient, as it is usually defined, always has the value of unity

$$\rho_1{}^2(\omega) = \frac{\left|\Phi_{ic}(j\omega)\right|^2}{\Phi_{ii}(\omega)\Phi_{cc}(\omega)} = \frac{F^*[i(t)]\,F[c(t)]\,F[i(t)]\,F^*[c(t)]}{F^*[i(t)]\,F[i(t)]\,F^*[c(t)]\,F[c(t)]} = 1$$

This result is now recognized to be true in the absence of smoothing. It is now suggested that the power-spectral density be smoothed over a finite frequency bandwidth. The modified definition of ρ then takes the form

$$\rho_2{}^2(\omega) = \frac{\left|\frac{1}{2K+1}\sum_{k=-K}^{K}\Phi_{ic}(j\omega + jk\Delta\omega)\right|^2}{\frac{1}{2K+1}\sum_{k=-K}^{K}\Phi_{ii}(\omega + k\Delta\omega)\,\frac{1}{2K+1}\sum_{k=-K}^{K}\Phi_{cc}(\omega + k\Delta\omega)}$$

$$= \frac{\left|\sum_{k=-K}^{K}F_k^*[i(t)]\,F_k[c(t)]\right|^2}{\sum_{k=-K}^{K}F_k^*[i(t)]\,F_k[i(t)]\sum_{k=-K}^{K}F_k^*[c(t)]\,F_k[c(t)]}$$

$$\neq 1$$

The linear correlation coefficient so defined is not, in general, equal to unity even for a linear system, contrary to popular belief. The coefficient does equal unity if the relationship between i and c is constant over the bandwidth, whether or not the system is linear. It is apparent, therefore, that a further improvement is needed. It is suggested that the linear correlation coefficient be expressed as

$$\rho_3{}^2(\omega) = \frac{\left|\sum_{n=1}^{N}F^*[i_n(t)]\left(F[c_n(t)]\right)\right|^2}{\sum_{n=1}^{N}F^*[i_n(t)]\,F[i(t)]\sum_{n=1}^{N}F^*[c_n(t)]\,F[c_n(t)]}$$

In this expression, an ensemble average is used instead of an average over a range in frequency. The result is that now only linear systems free of any stochastic signals will produce a value of unity, provided the input is not the same for each ensemble. In the event the input is the same, nonlinear systems will appear to be linear, with $\rho_3 = 1$.

Linear Time Domain Method

Let us now consider a linear analysis in the time domain in which the output of a linear pilot model is expressed in the form (see ref. 7)

$$c(t) = \int_0^{T_M} h_p(\tau)e(t-\tau)d\tau$$

Because the time histories c(t) and e(t) must be sampled for analysis, it is more appropriate to write

$$c(n) = \sum_{m=1}^{M} h_p(m)e(n - m + 1)$$

or in matrix form

$$\underline{c} = E\,\underline{h}_p$$

where

$$E = \begin{bmatrix} e(M) & e(M-1) & \cdots & e(3) & e(2) & e(1) \\ \cdot & & & e(4) & e(3) & e(2) \\ \cdot & & & & e(4) & e(3) \\ \cdot & & & & & e(4) \\ \cdot & & & & & \cdot \\ \cdot & & & & & \cdot \\ e(N-1) & & & & & e(N-M) \\ e(N) & e(N-1) & \cdots & & & e(N-M+1) \end{bmatrix}$$

$$\underline{h}_p = \begin{pmatrix} h_p(1) \\ h_p(2) \\ \cdot \\ \cdot \\ h_p(M) \end{pmatrix}$$

$$\underline{c} = \begin{pmatrix} c(M) \\ c(M+1) \\ \cdot \\ \cdot \\ c(N) \end{pmatrix}$$

The sampled impulse response of the pilot model, $h_p(m)$, can be obtained by using least squares

$$\underline{h}_p = [E^T E]^{-1} E^T \underline{c}$$

Inherent in the time domain representation of the pilot model is the assumption that the output at any one time is a function of only a finite time of the history of the error. The finite time period (or maximum memory) is denoted by T_M ($T_M = M\Delta\tau$) in the integral expression or M in the summation expression for the pilot model output. For the pilot model, T_M was varied (by changing $\Delta\tau$ and keeping M constant) until it was determined that the value of $h_p(\tau)$ was essentially zero beyond about 1 second. The value of T_M selected is somewhat larger than 1 second. Figure 5 shows an example result of such an analysis. It can be seen that the model impulse response first peaks at about 0.25 second, then reverses at about 0.45 second to peak in the opposite direction at about 0.6 second, then subsides to zero. The first sample (τ = 0.05 sec) is typically negative but has been faired to correspond to a pure time delay of 0.05 second. One indication of the degree to which a model represents an actual pilot is the ratio of the output of the power of the model in relation to the total power of the pilot's output. Linear pilot models will typically account for 65 to 90 percent of the total power of the output for a 4-minute run. The percentage is somewhat higher for shorter runs.

The time domain results can be transformed to the frequency domain for comparison with the frequency domain results through the use of the Fourier transform

$$\hat{Y}_p(j\omega) = F\left[\hat{h}_p(\tau)\right]$$

Figure 6 shows such a comparison. The agreement between the two methods is good. One advantage of the time domain method is that $\hat{Y}_p(j\omega)$ can be determined as a continuous function of frequency even when the input consists of sinusoids as it does for the example shown. The time domain results by their nature will always yield $\angle\hat{Y}_p(j\omega) = 0$, or -180°, as $\omega \longrightarrow 0$ and $\dfrac{d\left|\hat{Y}_p(j\omega)\right|}{d\omega} = 0$, as $\omega \longrightarrow 0$. Had the pilot describing function exhibited gain fluctuations or a phase lag at the lowest frequencies shown, these characteristics would not have been identified by the time domain model unless the value of T_M were increased considerably. This does not mean that the time domain model causes a restriction, but, rather, that T_M should not be unduly limited. Just as it is necessary to constrain the frequency domain model by smoothing, it is also necessary to constrain the time domain model by limiting T_M to a value considerably less than the record length. For pilot models, this represents a very natural and meaningful constraint in the time domain, compared with smoothing in the frequency domain. Still another advantage of analysis in the time domain is the capability of constructing nonlinear pilot models.

Nonlinear Time Domain Method

Nonlinear behavior on the part of the pilot accounts for at least part of the remnant of a linear pilot model. It is, therefore, of interest to investigate nonlinear pilot models. The output of a nonlinear time domain pilot model can be expressed by using a Volterra integral series

$$c(t) = \underbrace{\int_0^{T_M} h_{p_1}(\tau)e(t-\tau)d\tau}_{\text{(linear)}} + \underbrace{\int_0^{T_M}\int_0^{T_M} h_{p_2}(\tau_1,\tau_2)e(t-\tau_1)e(t-\tau_2)d\tau_1 d\tau_2}_{\text{(quadratic)}} + \underbrace{\int_0^{T_M}\int_0^{T_M}\int_0^{T_M} h_{p_3}(\tau_1,\tau_2,\tau_3)e(t-\tau_1)e(t-\tau_2)e(t-\tau_3)d\tau_1 d\tau_2 d\tau_3}_{\text{(cubic)}} + \underbrace{\cdots\cdots\cdots\cdots}_{\text{(higher order)}}$$

or in the discrete case

$$c(n) = \sum_{m=1}^{M} h_1(m)e(n - m + 1) \quad \text{(linear)}$$
$$+ \sum_{m_1=1}^{M} \sum_{m_2=1}^{M} h_2(m_1, m_2)e(n - m_1 + 1)e(n - m_2 + 1) \quad \text{(quadratic)}$$
$$+ \sum_{m_1=1}^{M} \sum_{m_2=1}^{M} \sum_{m_3=1}^{M} h_3(m_1, m_2, m_3)e(n - m_1 + 1)e(n - m_2 + 1)e(n - m_3 + 1) \quad \text{(cubic)}$$
$$+ \ldots\ldots\ldots\ldots\ldots \quad \text{(higher order)}$$

It was reasoned that the pilot's control response would be symmetrical so that only the first (linear) and third (cubic) terms were used. The algorithm used to perform the analysis was again based on a least-squares solution (ref. 7).

If

$$\underline{c} = E_{1,3}\underline{h}_{p_{1,3}}$$

where

$$\underline{c} = \begin{pmatrix} c(M) \\ c(M+1) \\ \vdots \\ c(N) \end{pmatrix}$$

$$\underline{h}_{p_{1,3}} = \begin{pmatrix} h_1(1) \\ h_1(2) \\ \vdots \\ h_1(M) \\ h_3(1,1,1) \\ h_3(1,1,2) \\ \vdots \\ h_3(1,1,M) \\ h_3(1,2,2) \\ \vdots \\ h_3(M,M,M) \end{pmatrix}$$

$$E_{1,3} = \begin{bmatrix} e(M) \ldots e(1) & (e(M)e(M)e(M)) \ldots (e(M)e(M)e(1)) & (e(M)e(M-1)e(M-1)) \ldots \\ e(M+1) \ldots e(2) & & (e(M)e(M-1)e(1)) \ldots (e(1)e(1)e(1)) \\ e(M+2) & & \\ e(M+3) & & \\ \vdots & & \\ \vdots & & \\ \vdots & & (e(N-M+1)^2 e(N-M)) \\ e(N) \ldots e(N-M+1) & (e(N)e(N)e(N-1)) \ldots & e(N-M+1)^3 \end{bmatrix}$$

Then

$$\hat{\underline{h}}_{p_{1,3}} = \left[E_{1,3}{}^T E_{1,3}\right]^{-1} E_{1,3}{}^T \underline{e}$$

It is difficult to present the results of such an analysis in a meaningful form, but it is instructive to look at an example step response. Figure 7 shows the response to (1) a step of very small amplitude so that only the linear term contributes significantly to the response, and (2) a large step. The responses have been normalized to the amplitude of the step inputs to facilitate comparison. The response of the pilot model to the larger step is slightly faster, has more overshoot, and has a lower steady-state gain. The inclusion of the cubic term increased the ratio of the power of the model output to the total power of the pilot output by only a few percent. This result would indicate the remnant to be largely stochastic as opposed to nonlinear and deterministic.

If the nonlinear model is expanded to include more samples of the cubic term and higher order terms, dimensionality will become a problem. One means of reducing the total dimension is offered by Balakrishnan (ref. 7) and Hsieh (ref. 8). Through the employment of the adjoint system of equations, a cubic weighting function of the form

$$h_{p_3}(\tau_1, \tau_2, \tau_3) = \int_0^L f_3(t-\tau) f_3(t-\tau_2) f_3(t-\tau_3) d\tau_1 d\tau_2 d\tau_3$$

is obtained. This equation reduces the weighting function of three variables to a single function of one variable. This technique has not yet been applied to the problem of identifying pilot models, and it is not known if the reduction in dimensionality justifies the added computation required.

Analysis of the Pilot's Output

It would be of interest to know what portion of the pilot's response is deterministic, but not linear, in order to assess the potential of a nonlinear pilot model in describing the pilot's output. It is known that at least part of the pilot's output is stochastic, since results of repeated experiments are never identical. It is possible to estimate the proportioning of the power of the pilot's output by examining the power-spectral density functions of both the pilot's output and its ensemble average. Both functions are shown in figure 8. The cross-hatched peaks in the graph show the amount of power associated with a linear response at the frequencies of the input. The shaded areas show the change

in the power as a result of ensemble averaging. Since the deterministic response would be unchanged by averaging, the shaded areas are an indication of the power associated with the stochastic portion of the pilot's output, which will not be accounted for by a deterministic model. The unshaded areas, then, are upper limits on the potential increase in power accounted for by using a nonlinear rather than linear pilot model.

The bar graph at the right of figure 8 shows the proportioning of the power of the pilot's output to be 91.7 percent linear (and time invariant), 4.5 percent stochastic, and 3.8 percent nonlinear and other types of responses. These results should not be generalized, since changes in the controlled element and input can cause a marked change in the proportioning of the power. It should also be noted that a small amount of power may be attributed to a nonlinearity that is significant in other aspects, such as limit cycles.

CONCLUDING REMARKS

A review of frequency and time domain methods of analysis shows that both methods require constraints on the freedom of the pilot models. The constraint in the time domain is more natural and straightforward than that of smoothing in the frequency domain. The two methods show good agreement for the linear model when the input disturbance function consists of sinusoids.

The inclusion of a cubic term in the time domain pilot model represents the first time the analysis has been applied to human response data. For the example discussed, only a few additional percent of the power of the remnant was accounted for by the addition of the cubic term. An investigation of the power-spectral density of an ensemble average of pilot output indicates the reason to be the largely stochastic nature of the remnant. The proportioning of the power of the pilot's output appears to be about 92 percent due to linear response, 4 percent due to stochastic response, and 4 percent due to nonlinear and other types of responses.

With this step toward the application of time domain methods of analyzing human control response, the work ahead holds much promise for the determination of more meaningful and useful pilot models.

APPENDIX A

COMPARISON OF TWO ESTIMATES OF CROSS-SPECTRAL DENSITY APPLIED TO RANDOM SIGNALS

Two samples of a random signal were used to test the equivalence of two estimates of cross-spectral density. Figure 9 shows time histories of the two samples for 250 of the 400 time points used. The cross-correlation function given by

$$R_{xy}(\tau) = \frac{1}{2T}\int_{-T}^{T} x(t)y(t+\tau)dt \approx \frac{1}{N}\sum_{n=1}^{N} x_n y_{n+m}$$

where

$$\tau = mh$$

$$h = \text{time interval}$$

was computed and is plotted in figure 10. The random nature of the signals is borne out by the erratic nature of the cross-correlation function.

Figures 11(a) and 11(b) show the real and imaginary parts of the cross-spectral density as estimated by two different expressions, as follows:

$$\bar{\Phi}_{xy_1}(j\omega) = F\left[R_{xy}(\tau)\right] \approx \frac{h}{N+1}\sum_{k=-N}^{N} e^{-j\omega kh}\sum_{n=-N/2}^{N/2} x_n y_{n+k}$$

and

$$\bar{\Phi}_{xy_2}(j\omega) = \frac{F^*[x]F[y]}{2T} \approx \frac{h}{N+1}\left(\sum_{n=-N/2}^{N/2} x_n e^{j\omega nh}\right)\left(\sum_{m=-N/2}^{N/2} Y_m e^{-jmh}\right)$$

The values obtained by using the preceding expressions were identical except for an occasional difference in the fourth significant figure.

One possible explanation why calculations made by other investigators resulted in a difference for the two estimates is the effect of using a limited number of values (lags) of the cross-correlation function. Figures 12(a) and 12(b) show the effect of using fewer lags than the maximum number possible (in this case, 400). As fewer lags are used, the estimate departs from the example for 400 lags, nullifying the equivalence of the two estimates.

Another possible explanation for an apparent difference in the two estimates could be the effect of smoothing shown in figures 13(a) and 13(b). If smoothing were used for $\bar{\Phi}_{xy_1}(j\omega) = F\left[R_{xy}(\tau)\right]$ and not for $\bar{\Phi}_{xy_2}(j\omega) = \frac{F^*[x]F[y]}{2T}$, the difference could

erroneously be interpreted as being caused by the form of the estimates of cross-spectral density.

In conclusion, the two forms of cross-spectral density estimates yield identical results if (1) the number of "lags" is not limited, and (2) if identical smoothing is used in both bases.

APPENDIX B

EQUIVALENCE OF TWO ESTIMATES OF CROSS-SPECTRAL DENSITY

Consider the following sample time histories:

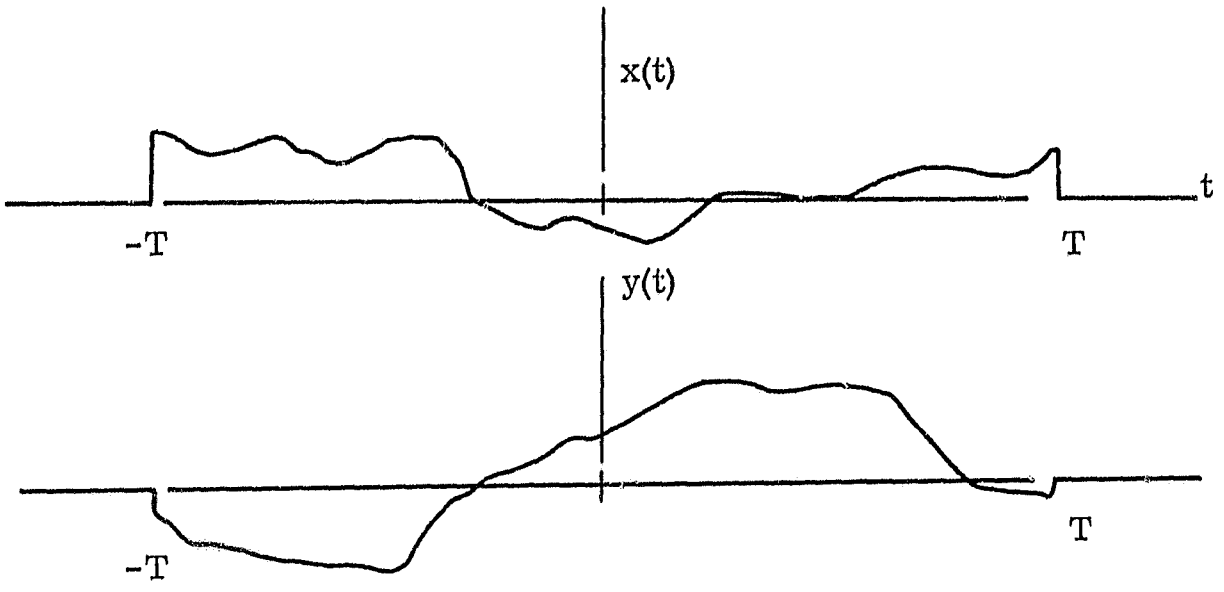

$$x(t) = 0 \quad \text{for} \quad t > T \quad \text{and} \quad t < -T$$

$$y(t) = 0 \quad \text{for} \quad t > T \quad \text{and} \quad t < -T$$

An estimate of the cross-correlation function can be expressed as

$$^{\dagger}R_{xy}(\tau) = \frac{1}{2T}\int_{-T}^{T} x(t)y(t+\tau)dt$$

and the Fourier transforms by

$$F[x] = \int_{-T}^{T} e^{-j\omega t}x(t)dt$$

$$F[y] = \int_{-T}^{T} e^{-j\omega t}y(t)dt$$

---

†Another estimate of $R_{xy}(\tau)$ involves division by $2T - \tau$ instead of $2T$, but the expression shown is usually more desirable.

APPENDIX B

The most popular estimate of the cross-spectral density function is the Fourier transform of the cross-correlation function

$$\hat{\Phi}_{xy_1}(j\omega) = F\left[R_{xy}(\tau)\right] = \int_{-2T}^{2T} e^{-j\omega\tau} \frac{1}{2T} \int_{-T}^{T} x(t)y(t+\tau)dtd\tau$$

An alternate and equivalent estimate is the product of two Fourier transforms

$$\hat{\Phi}_{xy_2}(j\omega) = \frac{F^*[x]\,F[y]}{2T} = \frac{1}{2T} \int_{-T}^{T} x(t)e^{j\omega t}dt \int_{-T}^{T} y(\alpha)e^{-j\omega\alpha}d\alpha$$

in which $F^*[\ ]$ denotes the complex conjugate of $F[\ ]$.

It is now desired to show that the two estimates are equal. This is done by substituting a change in variables and rearranging terms. Let $\alpha = \tau + t$ and substitute $\tau = \alpha - t$ in the expression of the first estimate

$$\hat{\Phi}_{xy_1}(j\omega) = \frac{1}{2T} \int_{-2T+t}^{2T+t} \int_{-T}^{T} e^{-j\omega(\alpha-t)} x(t)y(\alpha)dtd\alpha$$

Examination of the values for which $x(t)$ and $y(\tau)$ and $y(\alpha)$ are zero enables the limits of integration to be simplified as illustrated in the following figure. Before the change of variable, the combinations of t and τ for which the integrand is not necessarily zero are represented by the shaded area. Because $x(t)$ and $y(\tau)$ are zero for t, $\tau > T$, or $> -T$, the integrand is necessarily zero outside the shaded area.

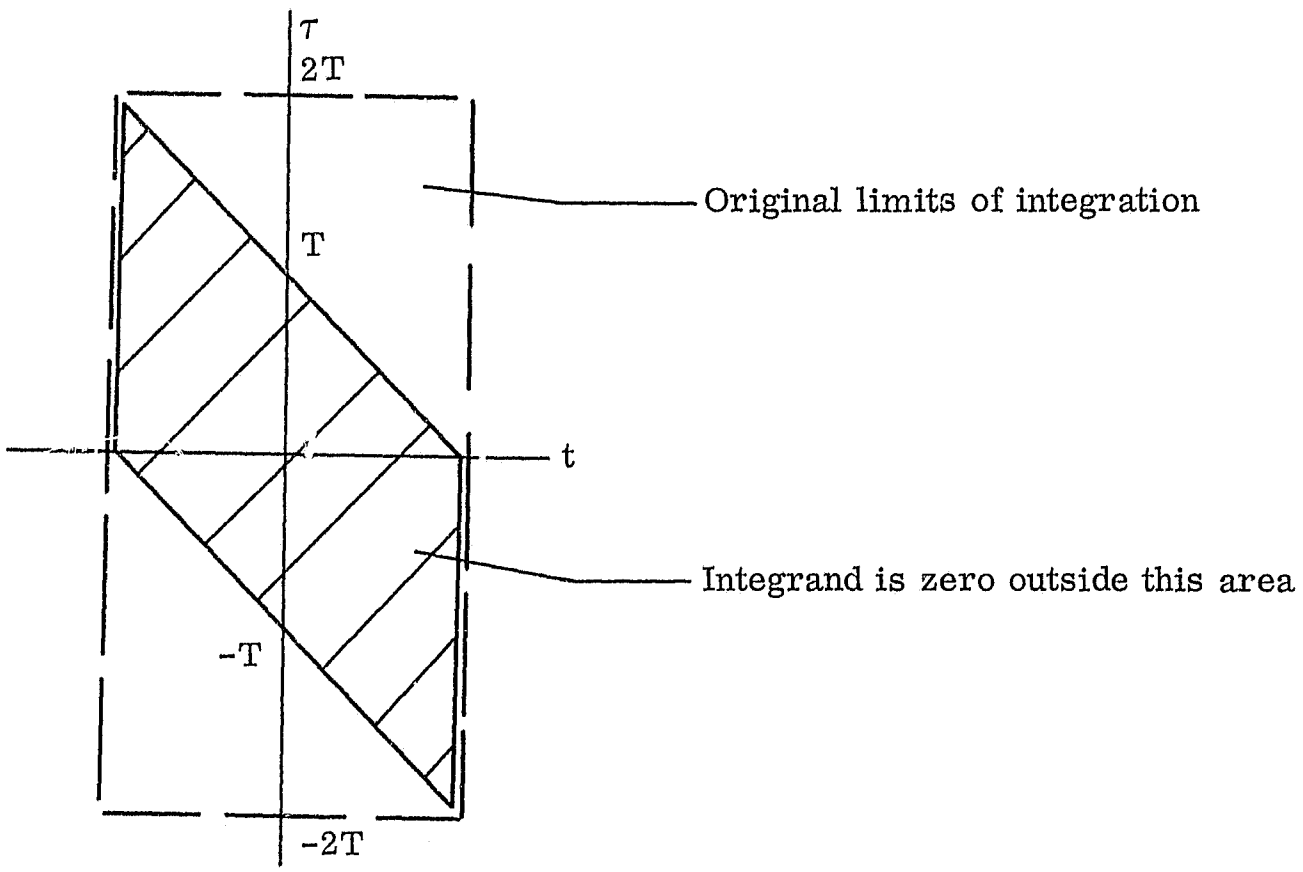

APPENDIX B

After the change in variable, the same area is transformed to that shown in the following figure:

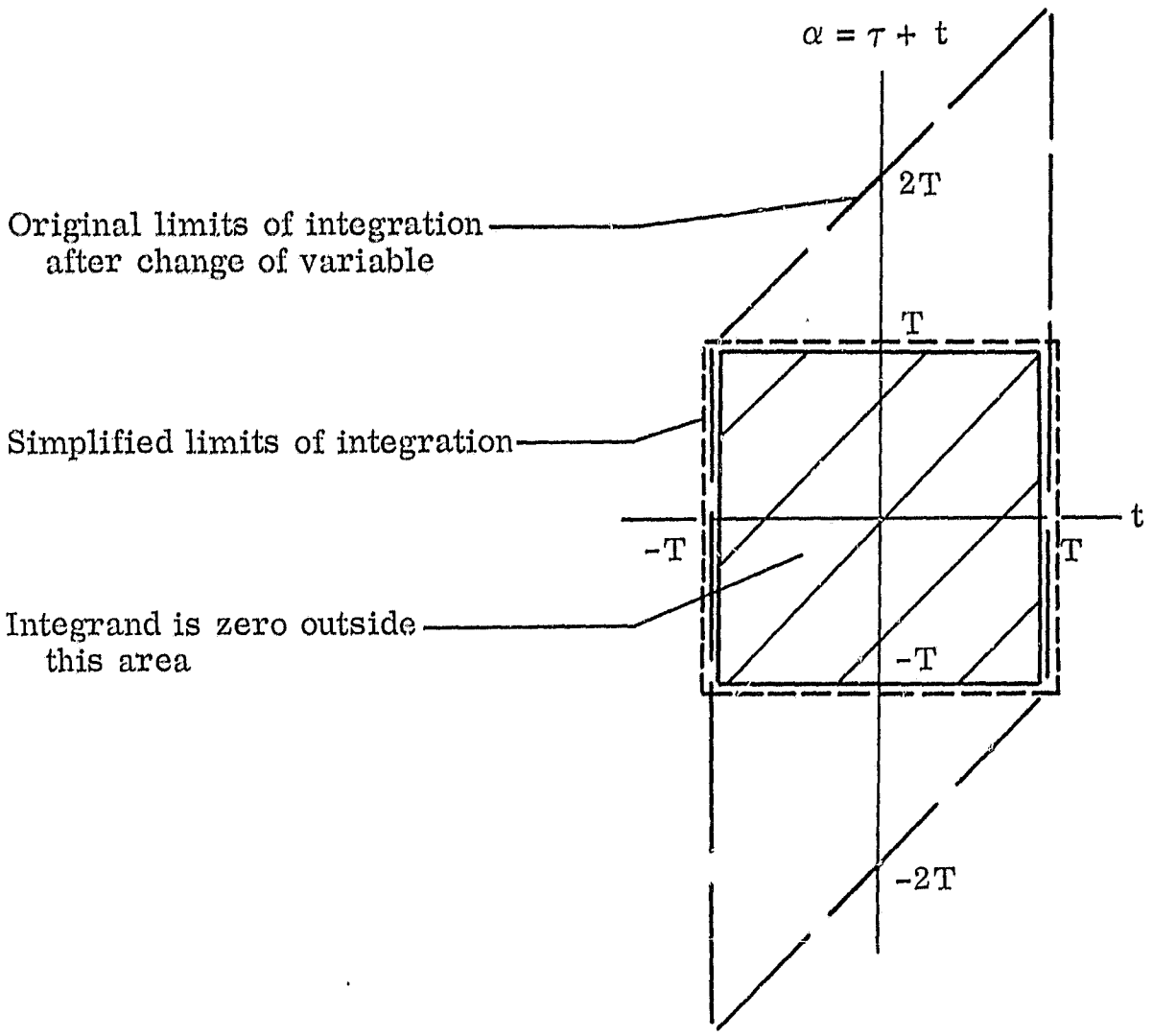

Superimposed on the same plot are the simplified limits of integration. These limits have no effect on the integral, since both sets of limits completely cover the area for which the integrand is not zero. Therefore

$$\Phi_{xy_1}(j\omega) = \frac{1}{2T} \int_{-T}^{T} \int_{-T}^{T} e^{-j\omega(\alpha - t)} x(t) y(\alpha) dt d\alpha$$

It is now possible to rearrange the expression to get

$$\Phi_{xy_1}(j\omega) = \frac{1}{2T} \left[\int_{-T}^{T} e^{j\omega t} x(t) \right] \left[\int_{-T}^{T} e^{-j\omega\alpha} y(\alpha) d\alpha \right]$$

This expression is recognized to be the second (postulated) estimate. Thus

$$\Phi_{xy_1} = \frac{1}{2T} F^*[x] F[y] = \Phi_{xy_2}$$

The two estimates of cross- (or power) spectral density are, therefore, equal.

A similar proof of the equivalence of the two estimates of cross- and power-spectral densities is offered for the sampled time histories where

$$F^*[x] = \int_{-T}^{T} x(t)e^{j\omega t}dt \approx \sum_{n=-N/2}^{N/2} x_n e^{j\omega nh}$$

$$F[y] = \int_{-T}^{T} y(\alpha)e^{-j\omega\alpha}d\alpha \approx \sum_{m=-N/2}^{N/2} y_m e^{-j\omega mh}$$

The second estimate of the cross-spectral density is then

$$\Phi_{xy_2}(j\omega) = \frac{1}{2T}F^*[x]F[y] \approx \frac{h}{N+1}\left[\sum_{n=-N/2}^{N/2} x_n e^{j\omega nh}\right]\left[\sum_{m=-N/2}^{N/2} y_m e^{-j\omega mh}\right]$$

The first estimate may be written in the form

$$\Phi_{xy_1}(j\omega) = F\left[R_{xy}(\tau)\right] = \sum_{k=-N}^{N} e^{-j\omega kh}\frac{h}{N+1}\sum_{n=-N/2}^{N/2} x_n y_{n+k}$$

Then, letting $m = k + n$, and substituting $k = m - n$

$$\Phi_{xy_1}(j\omega) = \frac{h}{N+1}\sum_{m=-N+n}^{N+n} e^{-j\omega(m-n)h}\sum_{n=-N/2}^{N/2} x_n y_m$$

Rearranging

$$\Phi_{xy_1}(j\omega) = \frac{h}{N+1}\sum_{n=-N/2}^{N/2} e^{j\omega nh}x_n \sum_{m=-N+n}^{N+n} e^{-j\omega mh}y_m$$

Since x_n and y_m equal zero for m, $n > N/2$, and $< -N/2$, the limits can be changed to $\pm N/2$. Therefore

$$\Phi_{xy_1}(j\omega) = \frac{h}{N+1}\sum_{n=-N/2}^{N/2} e^{j\omega nh}x_n \sum_{m=-N/2}^{N/2} e^{-j\omega mh}y_m = \Phi_{xy_2}$$

SYMBOLS

c	pilot output (control deflection), inches
$\overline{c^2}$	mean square or total power of c, inches^2
E	error matrix
e	error, radians
F[ ]	Fourier transform
h	time interval, seconds
h_p	impulse response of pilot, inches/radian
i	input (external disturbance function), radians
$j = \sqrt{-1}$	
K	maximum value of k
k	index for frequency
L	total record length, seconds
M	maximum value of m, $M = \frac{T_M}{\Delta\tau}$
m	index for the argument of h_p
N	maximum value of n
n	index for time
o	linear output of pilot model (control deflection), inches
$R_{xy}(\tau)$	cross-correlation function
r	remnant signal of pilot model (control deflection), inches
s	Laplace variable
T	one-half total record length, seconds
T_M	maximum memory time of the pilot model, seconds
t	time, seconds

W_k	weighting function
x, y	sample signals
$Y_c(j\omega)$	controlled element transfer function, radians/inch
$Y_p(j\omega)$	pilot describing function, inches/radian
α	time variable, seconds
ρ	linear correlation coefficient
ρ_a	average linear coherence
τ	argument of h_p, seconds
$\Delta\tau$	incremental value of τ, seconds
$\Phi_{xy}(j\omega)$	cross-spectral density of x(t) and y(t)
$\Phi_{xx}(\omega)$	power-spectral density of x(t)
ω	frequency, radians/second
$\Delta\omega$	incremental value of ω, radians/second
$\wedge$	estimate

Matrix notation:

(x), $\underline{x}$	column matrix
[X]	rectangular or square matrix
X^T	transpose
X^{-1}	inverse
*	complex conjugate

Numbers used as subscripts denote the pertinent term or terms of the Volterra integral series or summation.

REFERENCES

1. McRuer, Duane; Graham, Dunstan; Krendel, Ezra; and Reisener, William, Jr.: Human Pilot Dynamics in Compensatory Systems. Tech. Rep. AFFDL TR-65-15, U.S. Air Force, July 1965.

2. Seckel, Edward; Hall, Ian, A. M.; McRuer, Duane T.; and Weir, David H.: Human Pilot Dynamic Response in Flight and Simulator. Tech. Rep. 57-520 (ASTIA No. AD130988), Wright Air Dev. Center, U.S. Air Force, Aug. 1958.

3. Smith, Harriet J.: Human Describing Functions Measured in Flight and on Simulators. Proceedings of Second NASA-University Conference on Manual Control, NASA SP-128, 1967.

4. Graham, Dunstan; and McRuer, Duane: Analysis of Nonlinear Control Systems. John Wiley & Sons, Inc., 1961.

5. James, H. M.; Nichols, N. B.; and Phillips, R. S.: Theory of Servomechanisms. McGraw-Hill Book Co., Inc., 1947.

6. Taylor, Lawrence W., Jr.: Discussion of Spectral Human Response Analysis. Proceedings of Second NASA-University Conference on Manual Control, NASA SP-128, 1967.

7. Balakrishnan, A. V.: Determination of Nonlinear Systems From Input-Output Data. Papers Presented at 54th Meeting of the Princeton University Conference on Identification Problems in Communication and Control Systems, March 21-22, 1963, Princeton University, 1963, pp. 31-49.

8. Hsieh, H. C.: An On-line Identification Scheme for Multivariable Nonlinear Systems. Computing Methods in Optimization Problems, A. V. Balakrishnan and Lucien W. Neustadt, eds., Academic Press (New York), 1964, pp. 193-210.

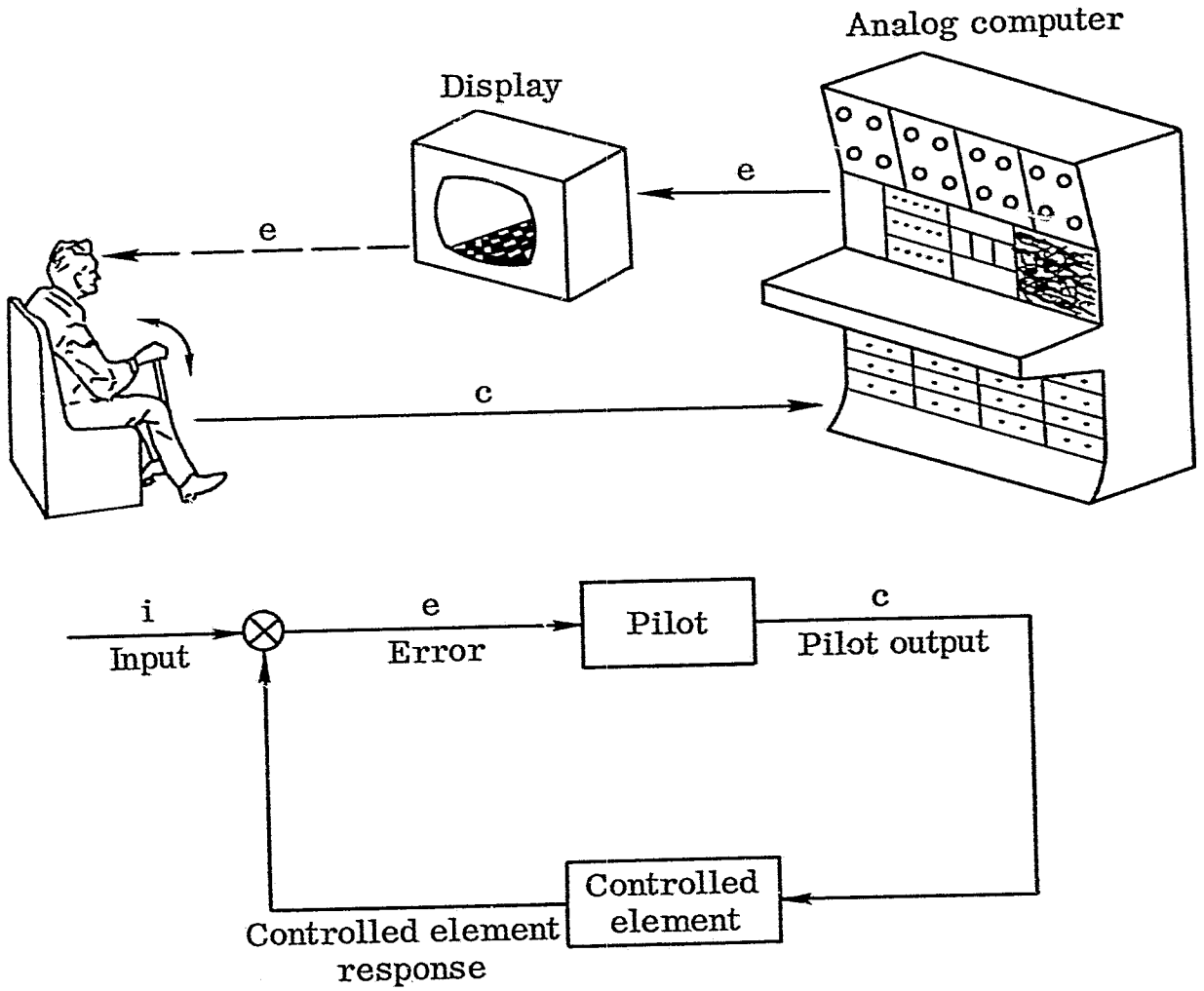

Figure 1.—Block diagram of a pilot in a compensatory tracking task.

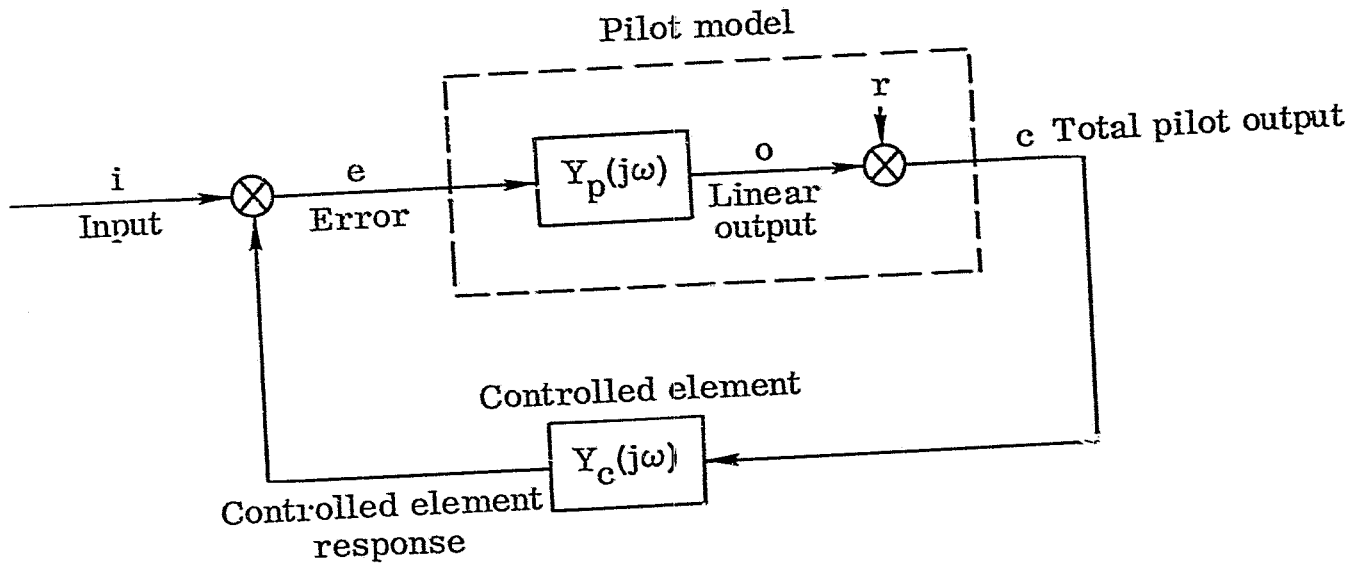

Figure 2.– Frequency domain model of a pilot.

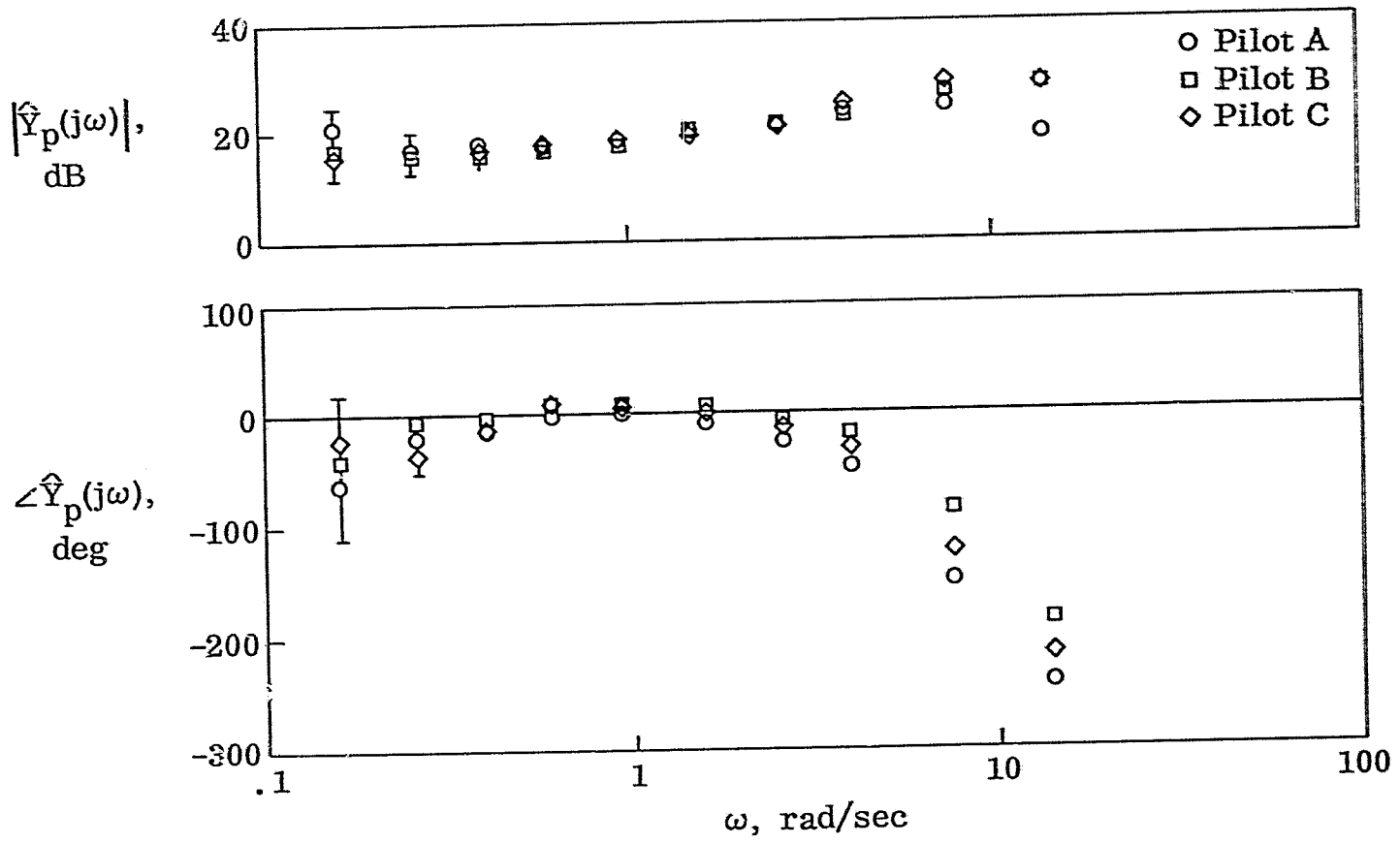

Figure 3.– Example of frequency domain model results. $Y_c \approx \frac{0.782}{s\left(s + \frac{1}{0.389}\right)}$.

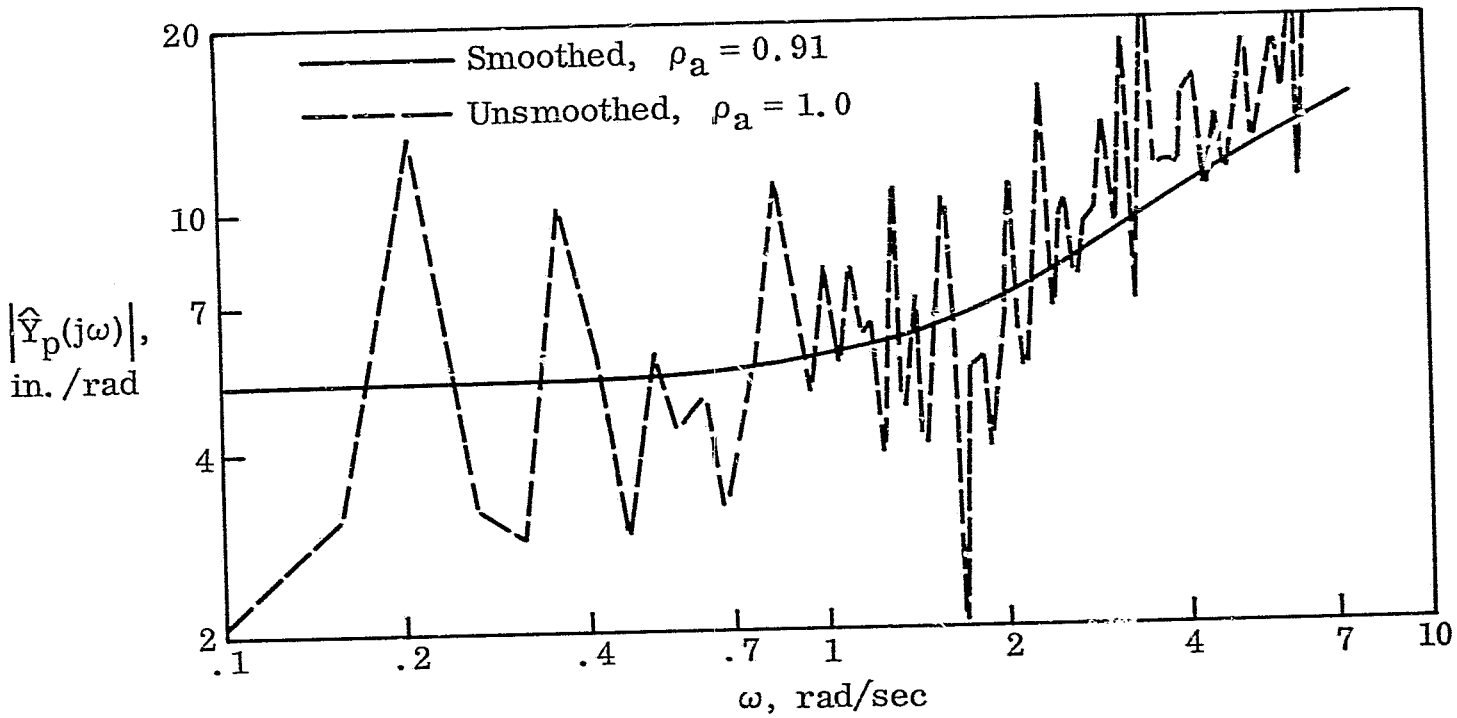

Figure 4. – Effect of smoothing the pilot describing function. $Y_c \approx \dfrac{0.782}{s\left(s + \dfrac{1}{0.389}\right)}$.

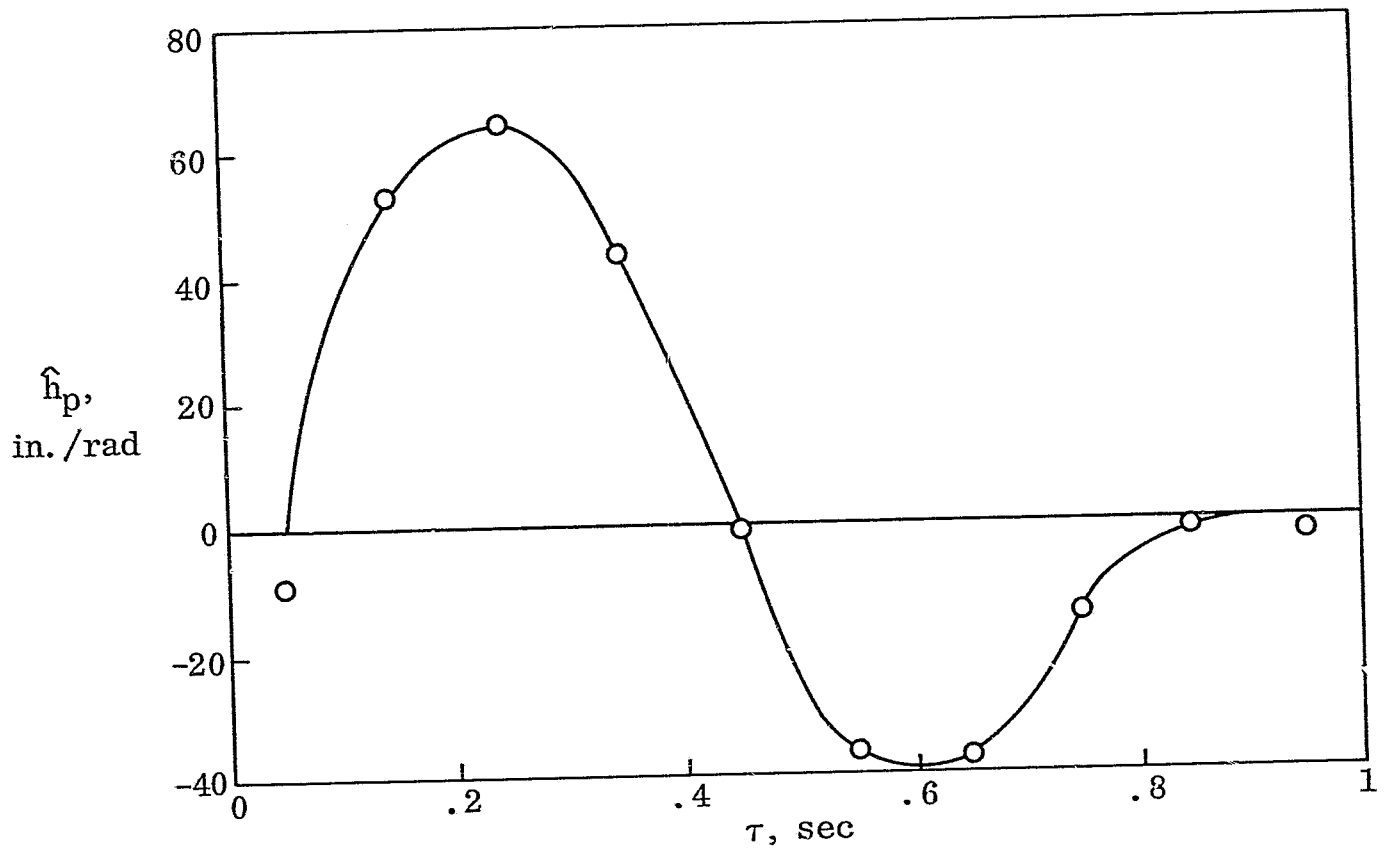

Figure 5. – Linear time domain model of the pilot. $Y_c \approx \frac{0.782}{s\left(s + \frac{1}{0.389}\right)}$.

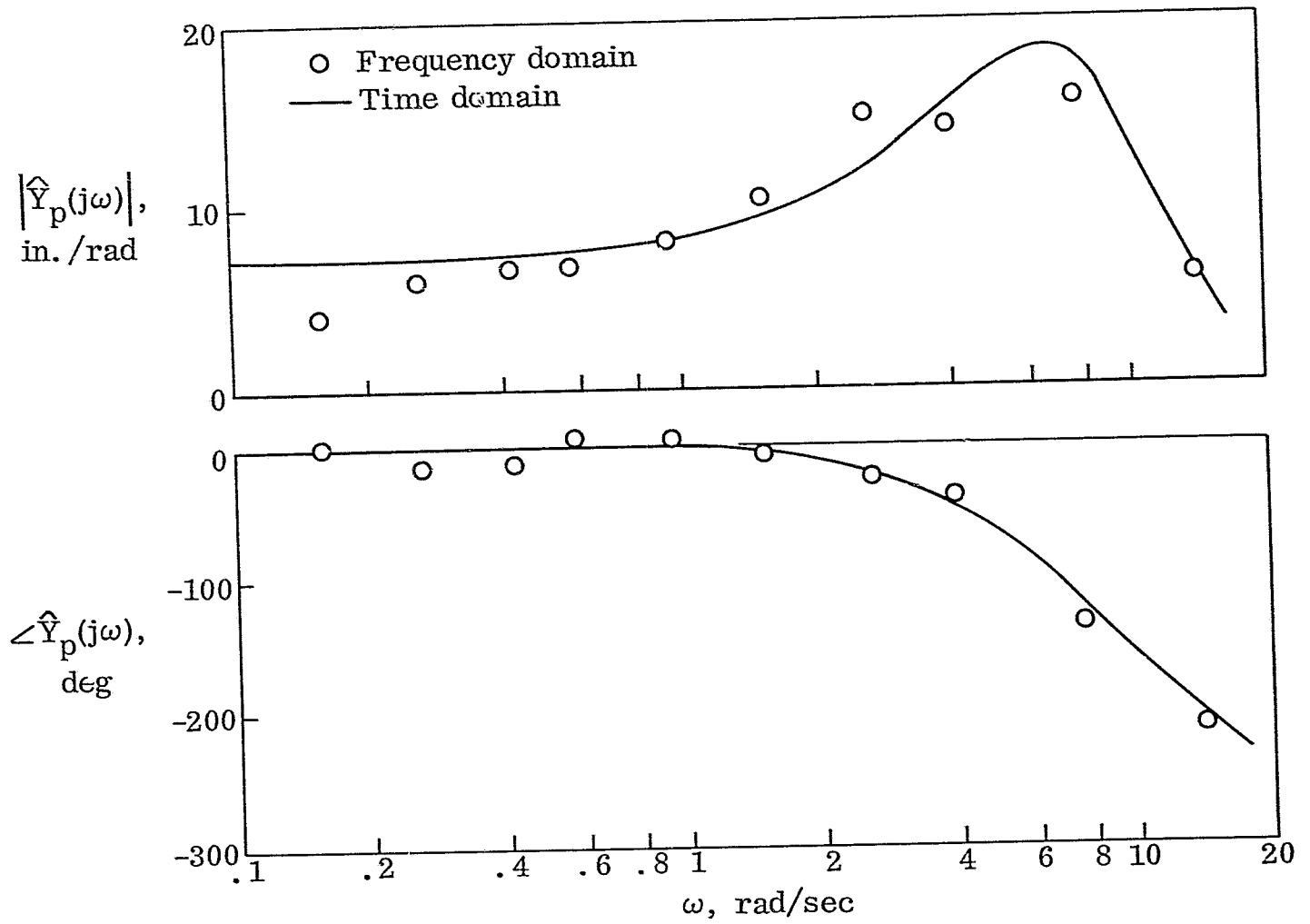

Figure 6.– Comparison of frequency and time domain models. $Y_c \approx \frac{0.782}{s\left(s + \frac{1}{0.389}\right)}$.

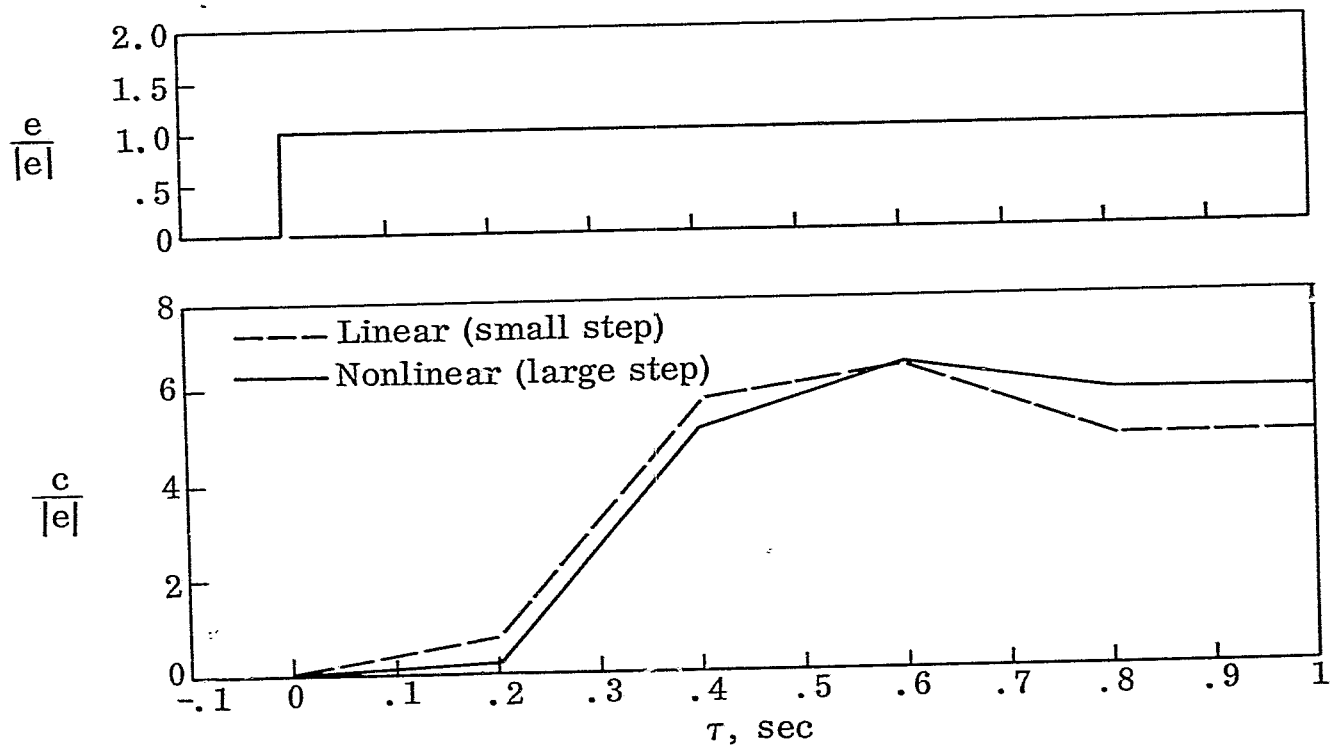

Figure 7. – Step responses of the nonlinear time domain pilot model. $Y_c = \frac{4.4}{s}$.

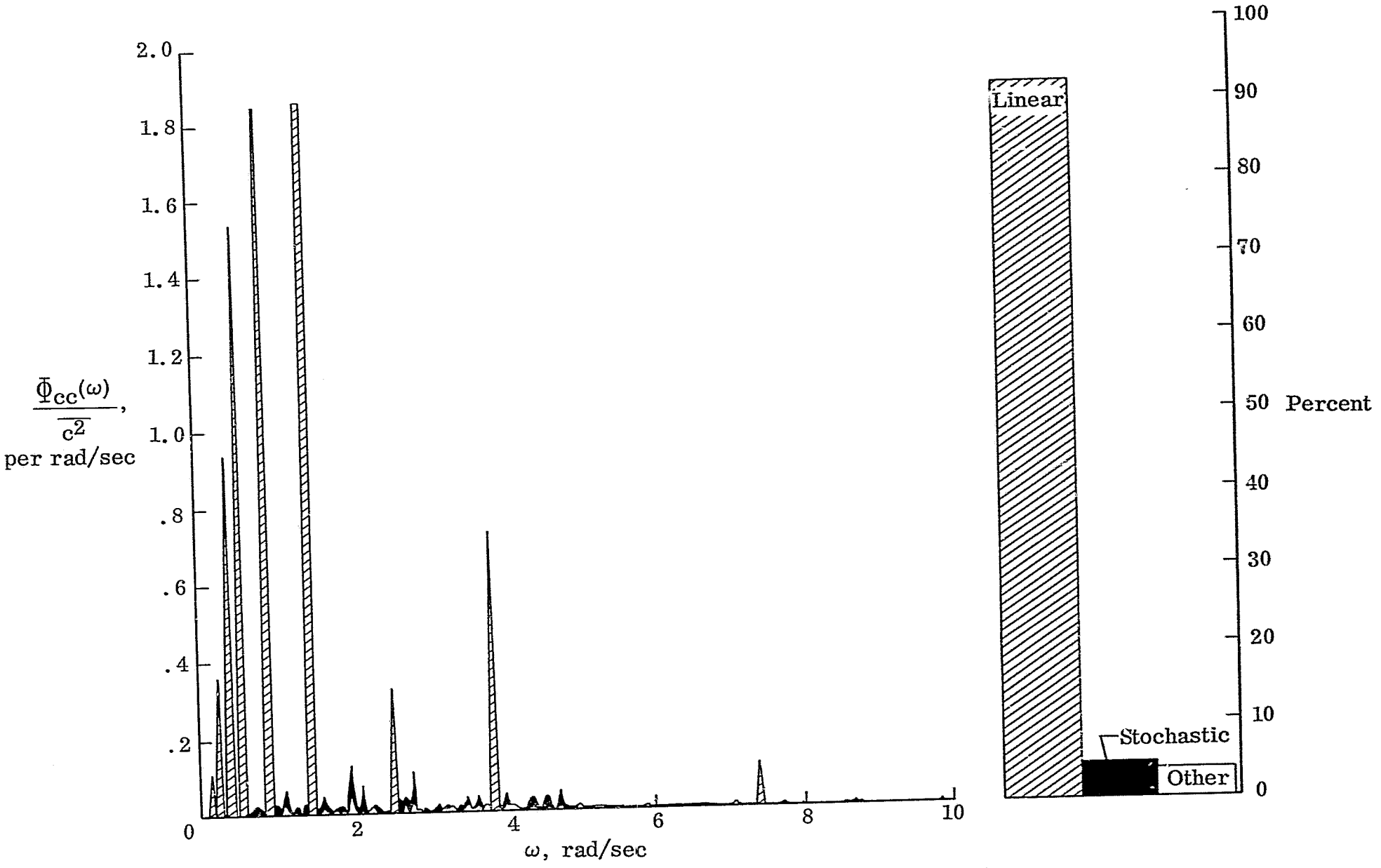

Figure 8.– Spectral analysis of pilot's output. $Y_c = \frac{4.4}{s}$.

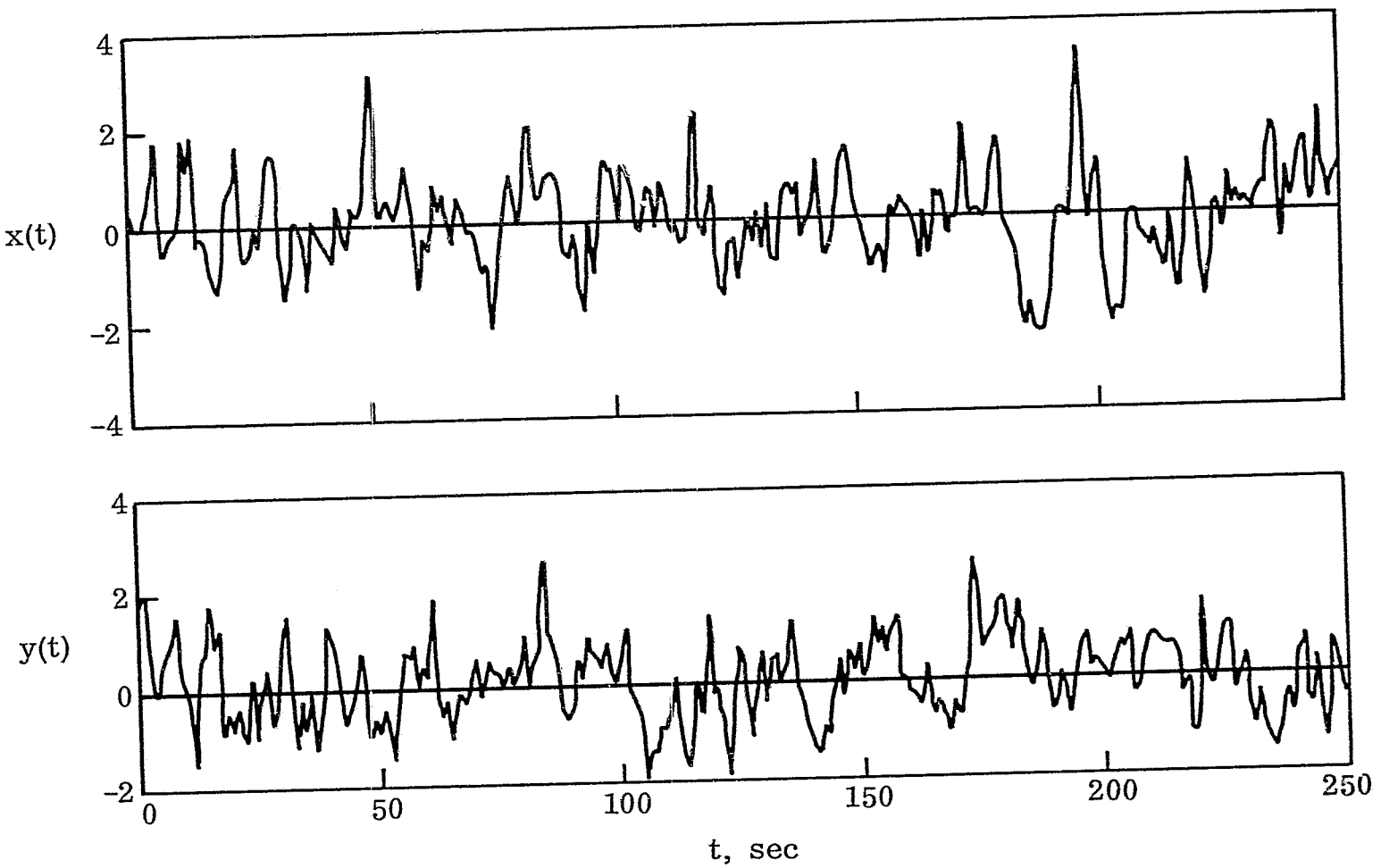

Figure 9. – Time histories of two independent random signals.

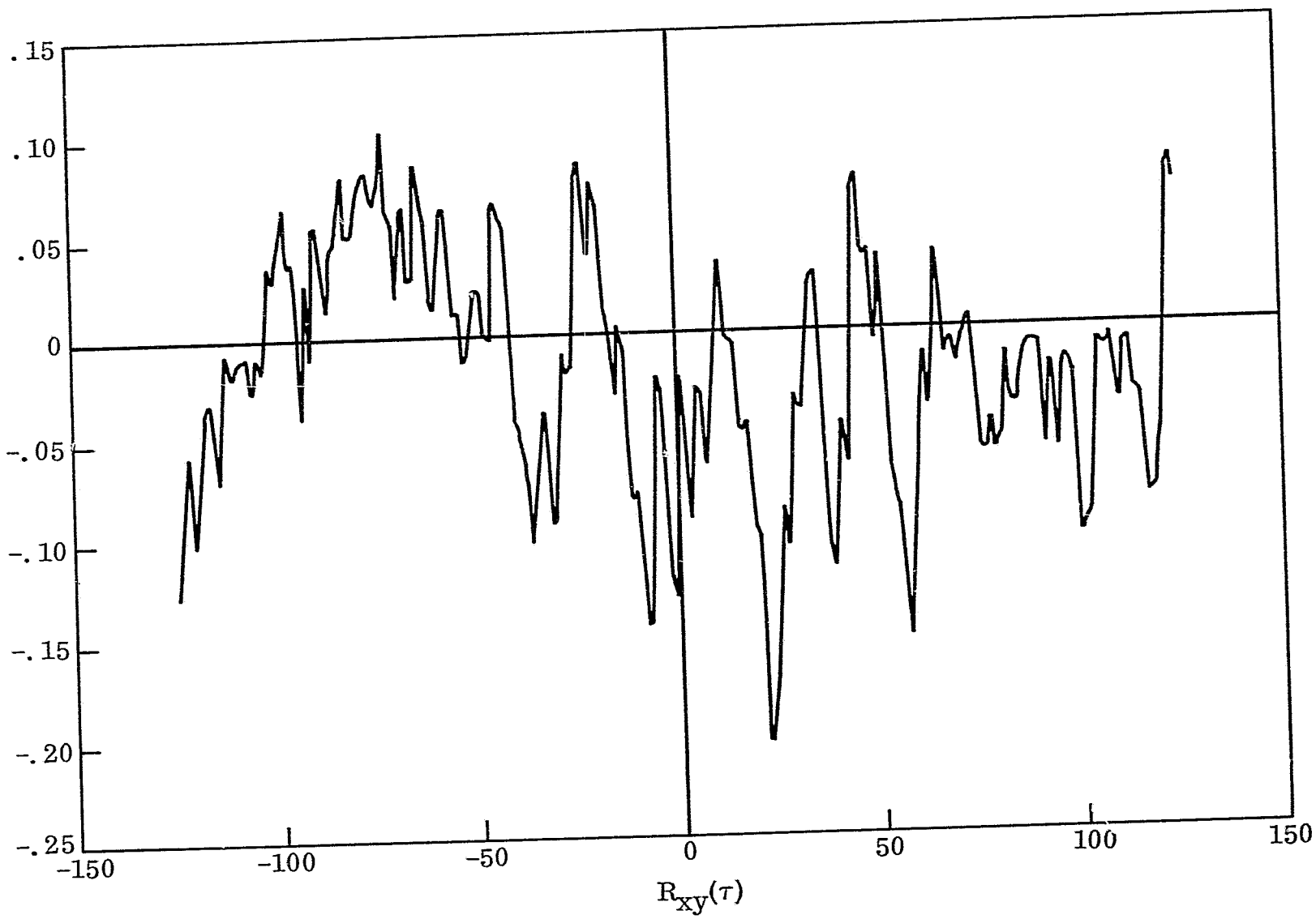

Figure 10.– Cross-correlation function of two random variables.

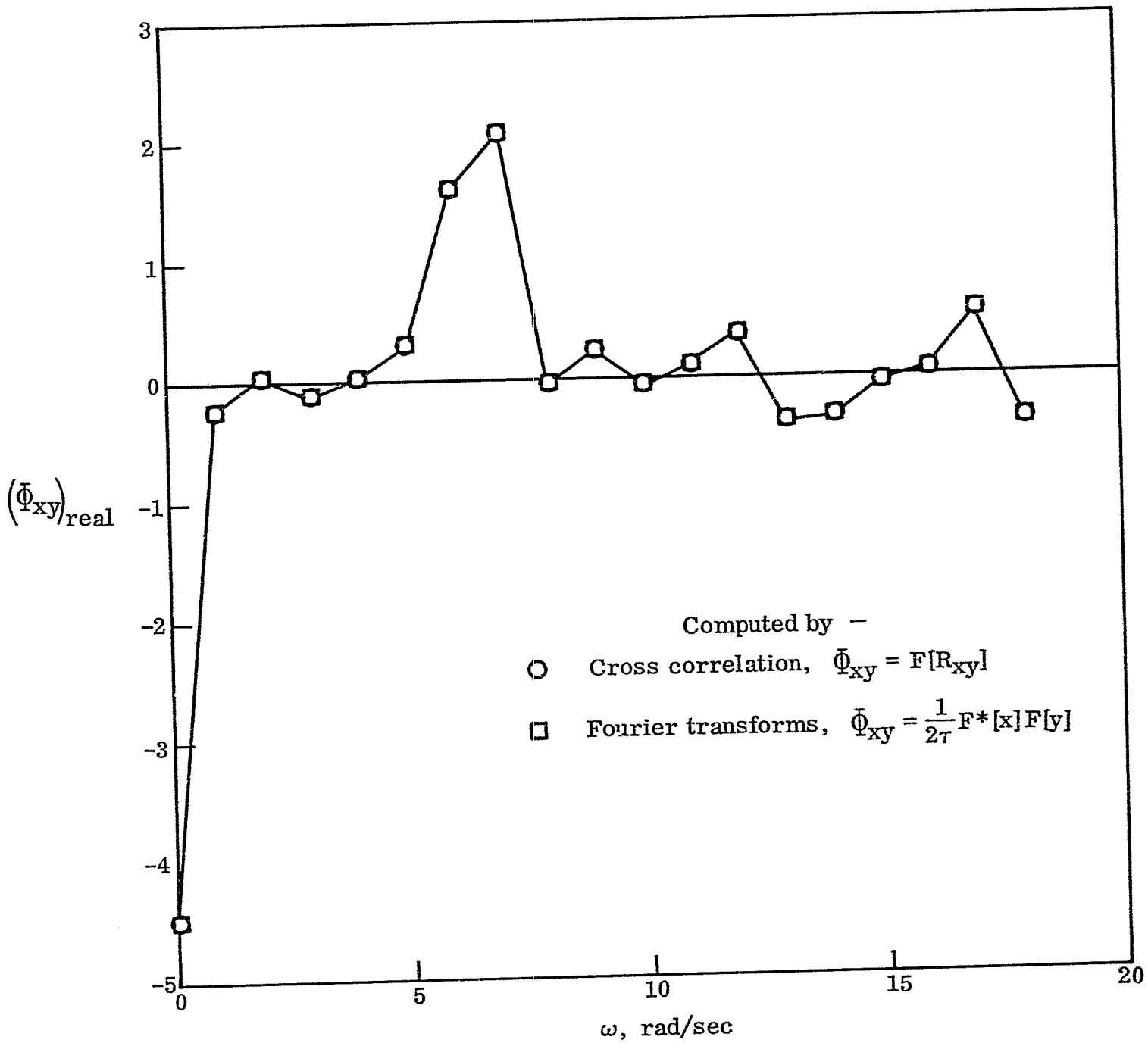

(a) Real parts.

Figure 11.– Comparison of cross spectra computed two different ways.

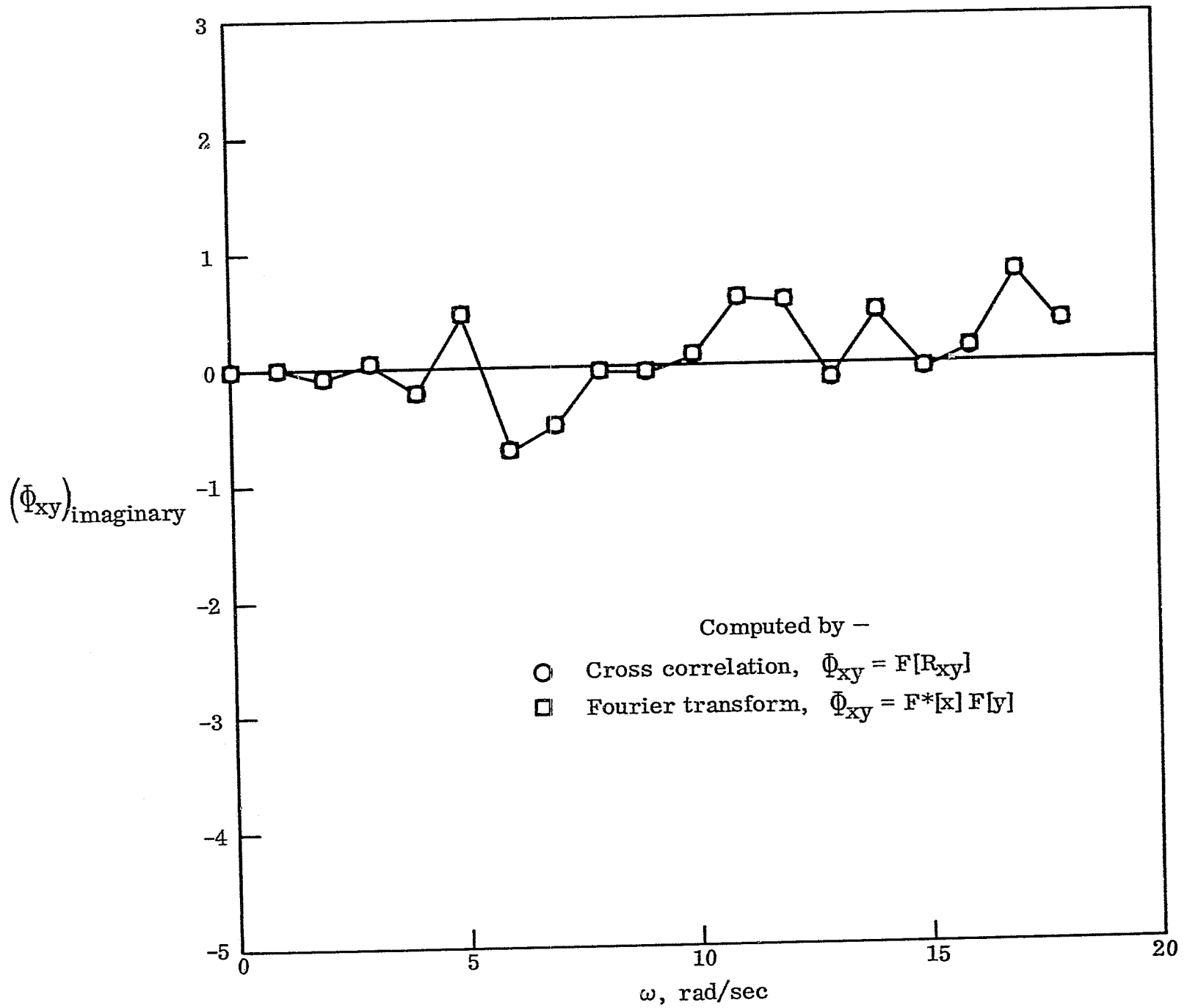

(b) Imaginary parts.

Figure 11.– Concluded.

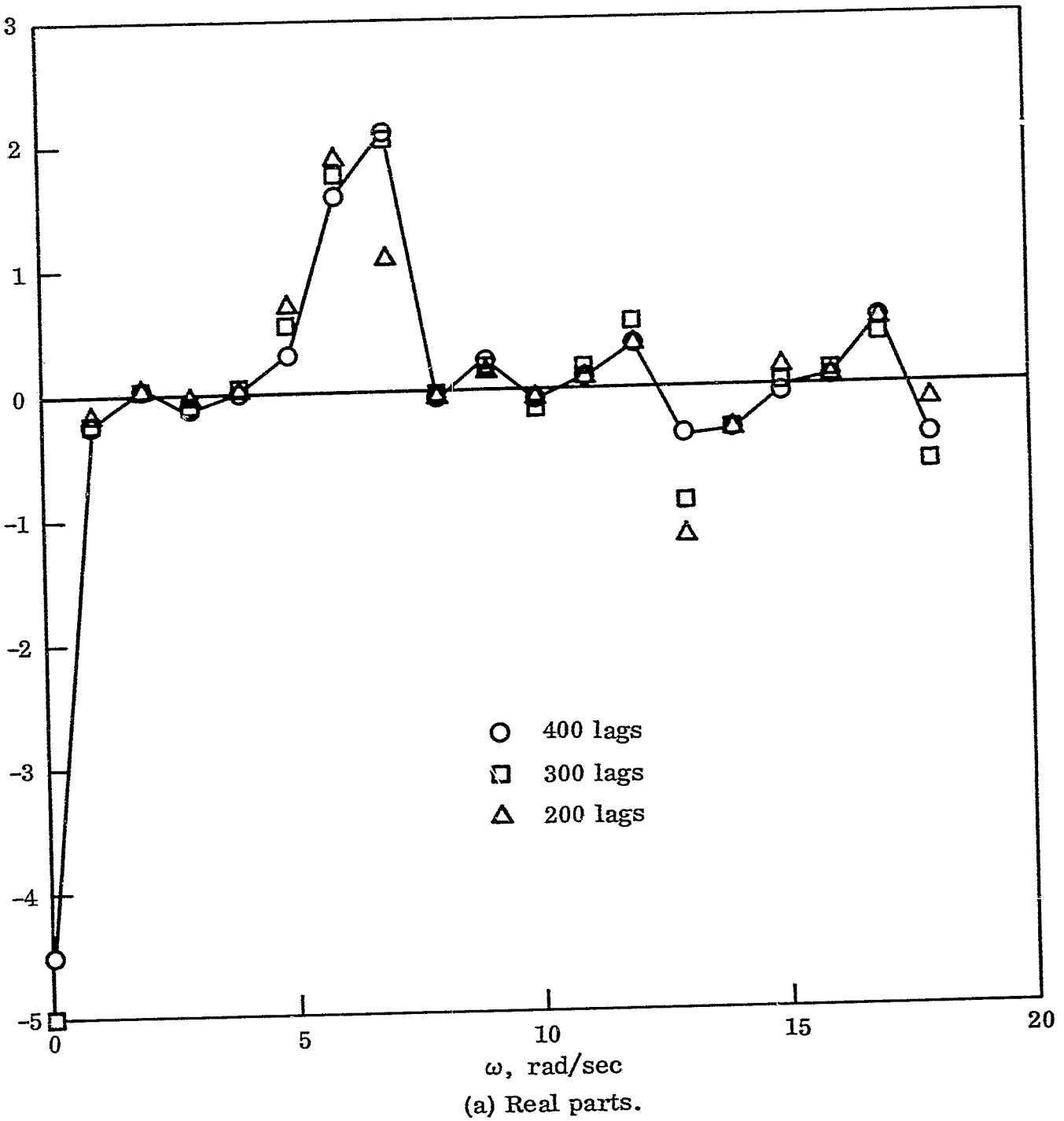

(a) Real parts.

Figure 12.– Effect of number of "lags" on the estimate of cross spectra.

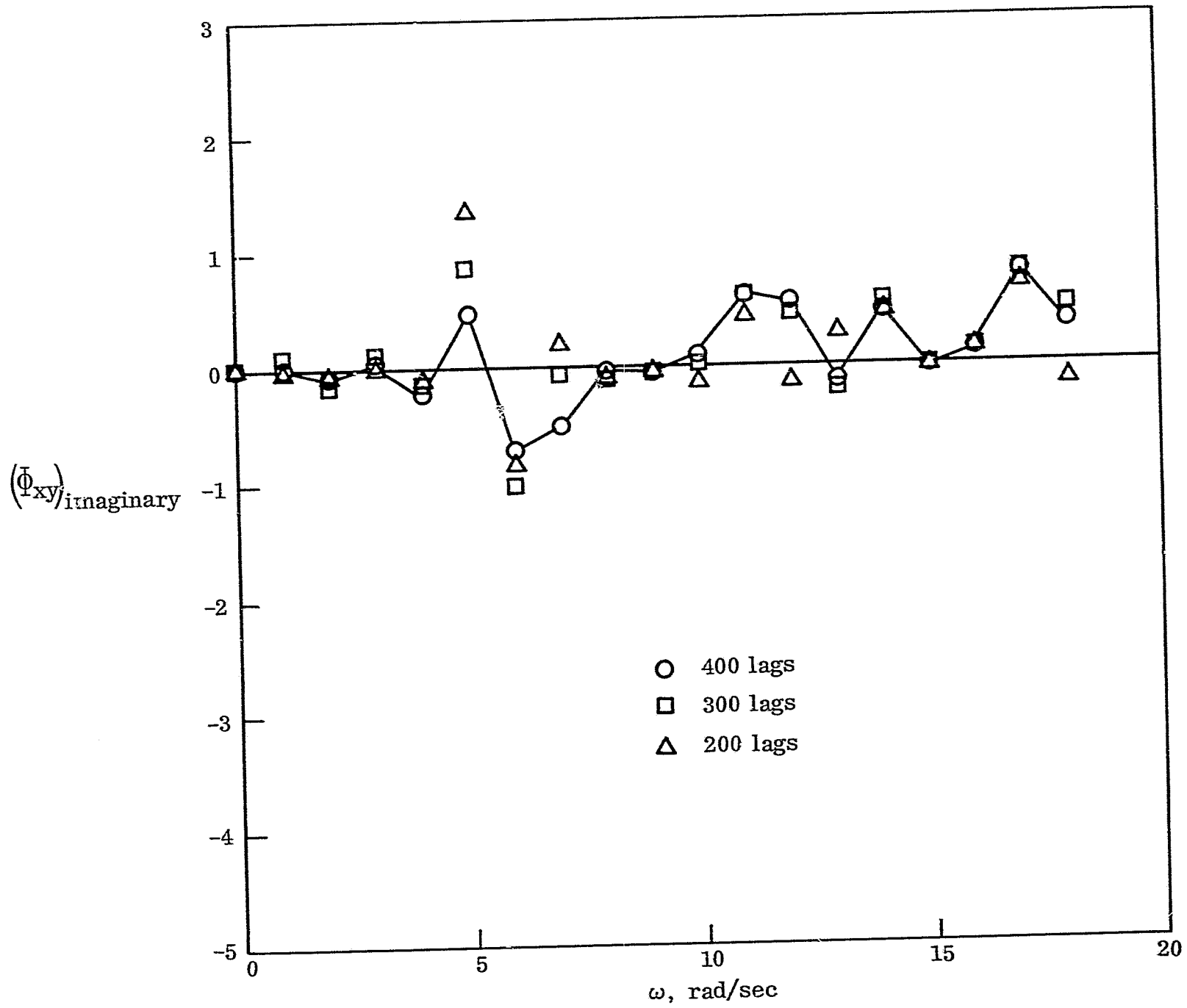

(b) Imaginary parts.

Figure 12. – Concluded.

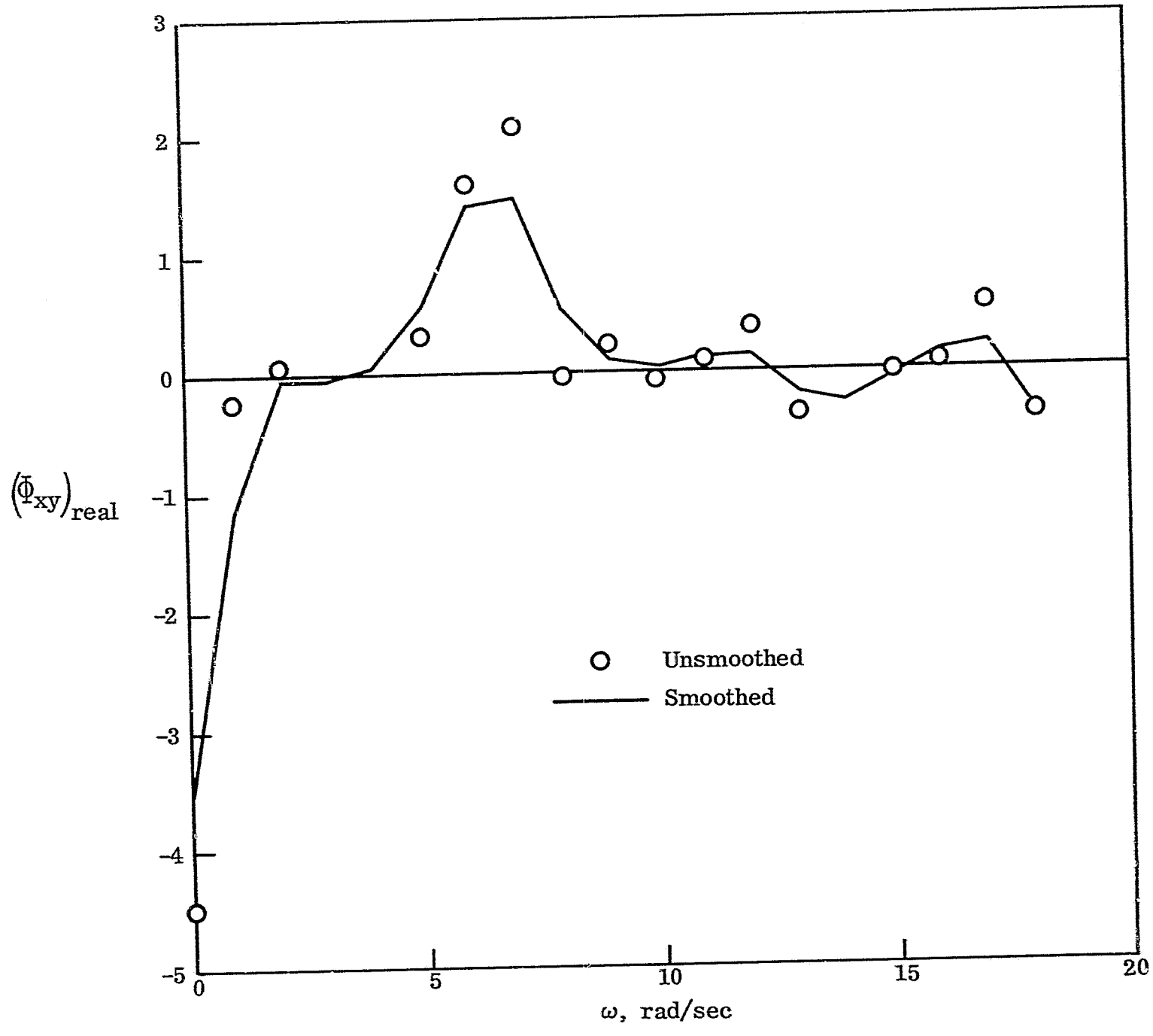

(a) Real parts.

Figure 13.– Effect of smoothing on cross-spectra estimates.

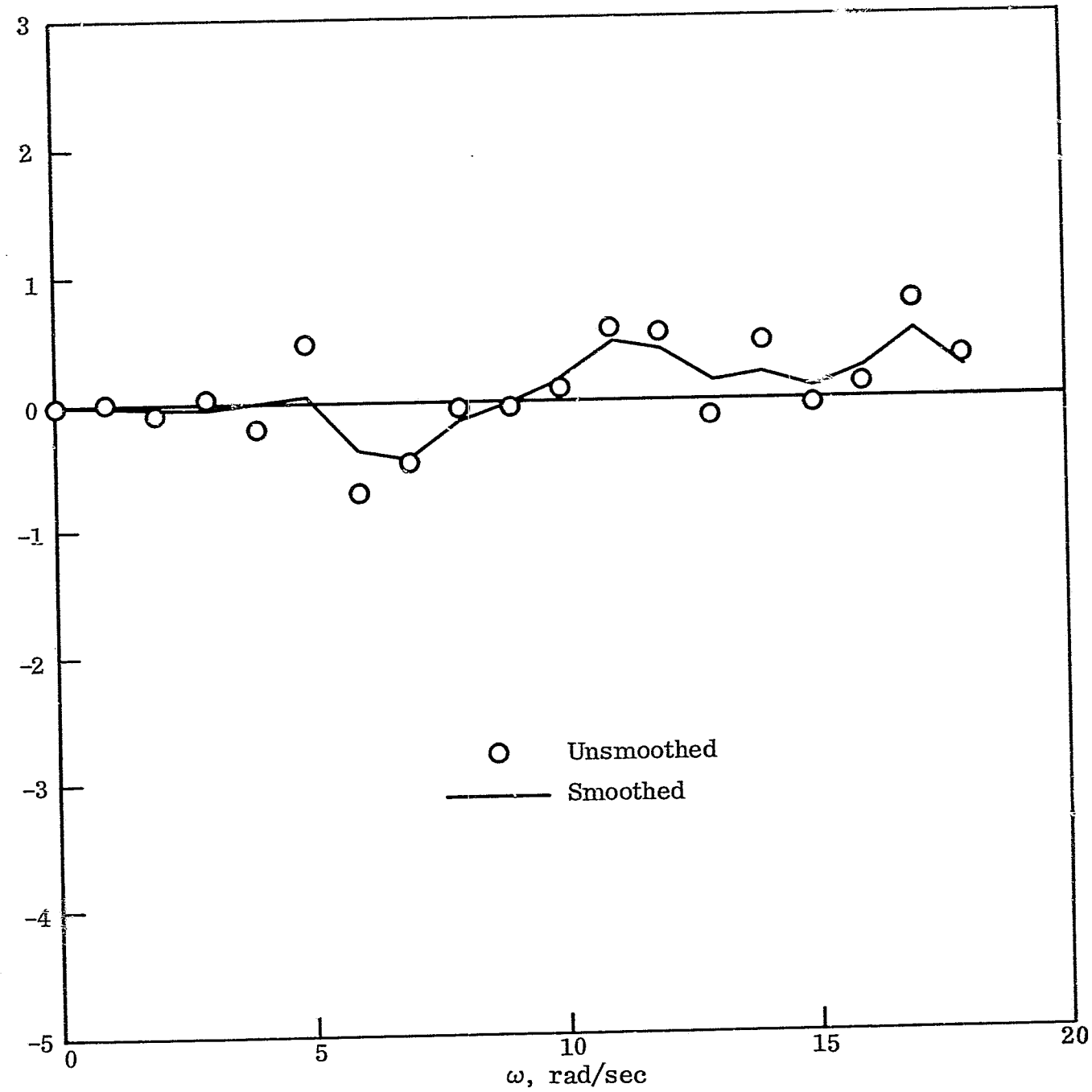

(b) Imaginary parts.

Figure 13. – Concluded.